Supporting information

Highly stable ladder-type conjugated polymer based organic electrochemical transistors for low power and signal processing-free surface electromyogram triggered robotic hand control

Zhongliang Zhou[1], Xihu Wu[1], Teck Lip Dexter Tam[2], Cindy G. Tang[1], Shuai Chen[1], Kunqi Hou[1], Ting Li[1], Qiang He[1], Ji-Jon Sit[1], Jianwei Xu[3] and Wei Lin Leong[1]*

[1]School of Electrical and Electronic Engineering, Nanyang Technological University,50 Nanyang Avenue, Singapore 639798, Singapore

E-mail: wlleong@ntu.edu.sg

[2]Institute of Sustainability for Chemical, Energy and Environment (ISCE2), Agency of Science, Technology and Research (A*STAR), 1 Pesek Road, Singapore 627833, Singapore

[3]Department of Chemistry, National University of Singapore, 3 Science Drive 3, Singapore 117543, Singapore.

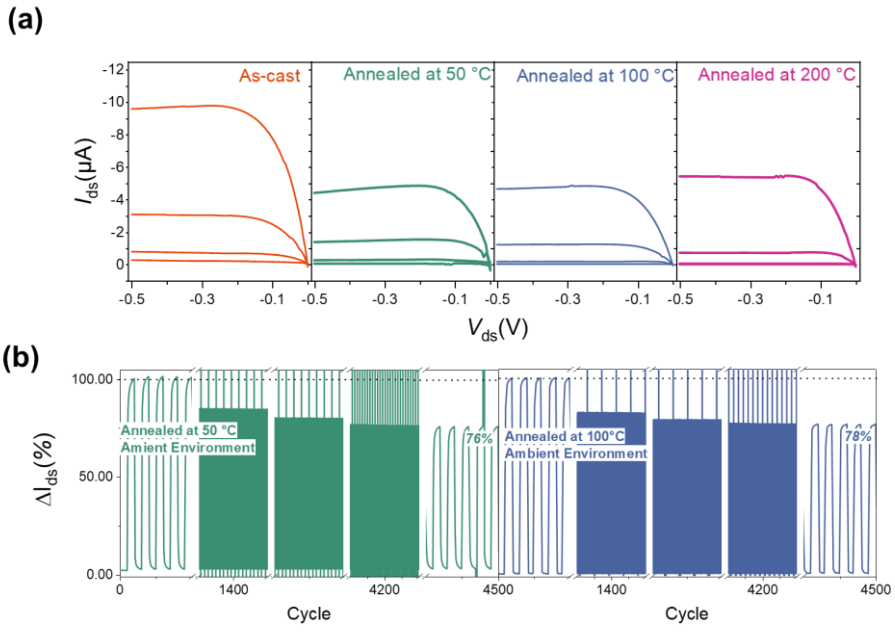

Figure S1 (a) Output curves of 4 PBBTL-based OECTs under different thermal annealing temperatures. (b) Pulse stability of OECTs annealed at 50 °C and 100 °C under ambient environment.

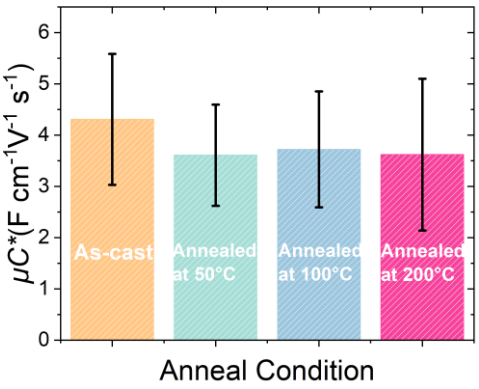

Figure S2 μC^* product at four different thermal annealing conditions, where the μC^* was calculated from g_m vs V_{gs} through linear fitting.

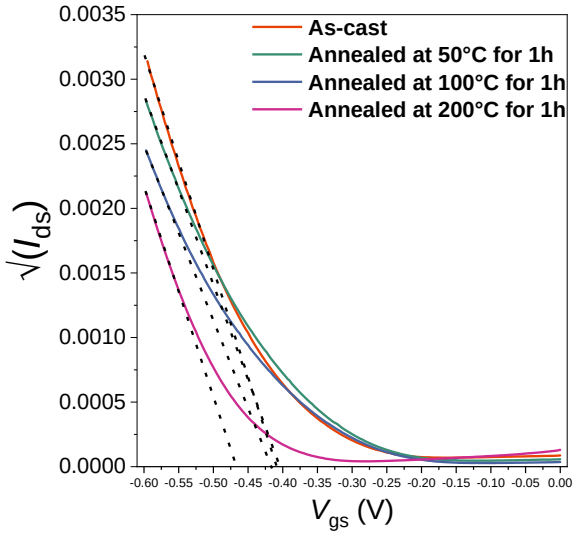

Figure S3 Linear fitting using $\sqrt{I_{ds}}$ vs. V_{gs} to extract the V_{th} under different annealing temperatures at a constant V_{ds} = -0.6V.

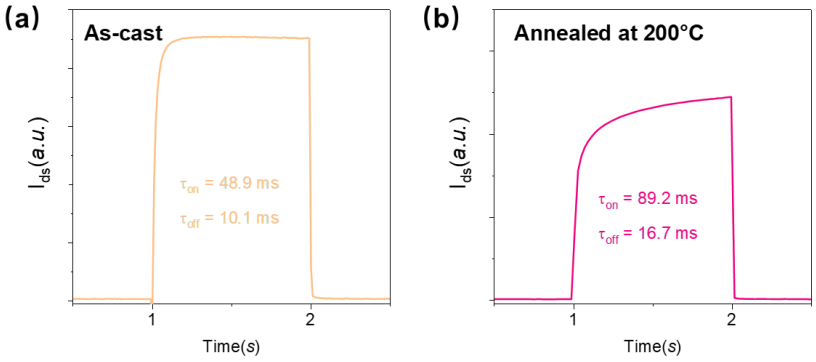

Figure S4 Switch speed of as-cast and annealed OECT at 200 °C, with pulsing V_{gs} varies from

0 V to -0.6 V (1 s, 50% duty cycle) and a constant V_{ds} of -0.6V.

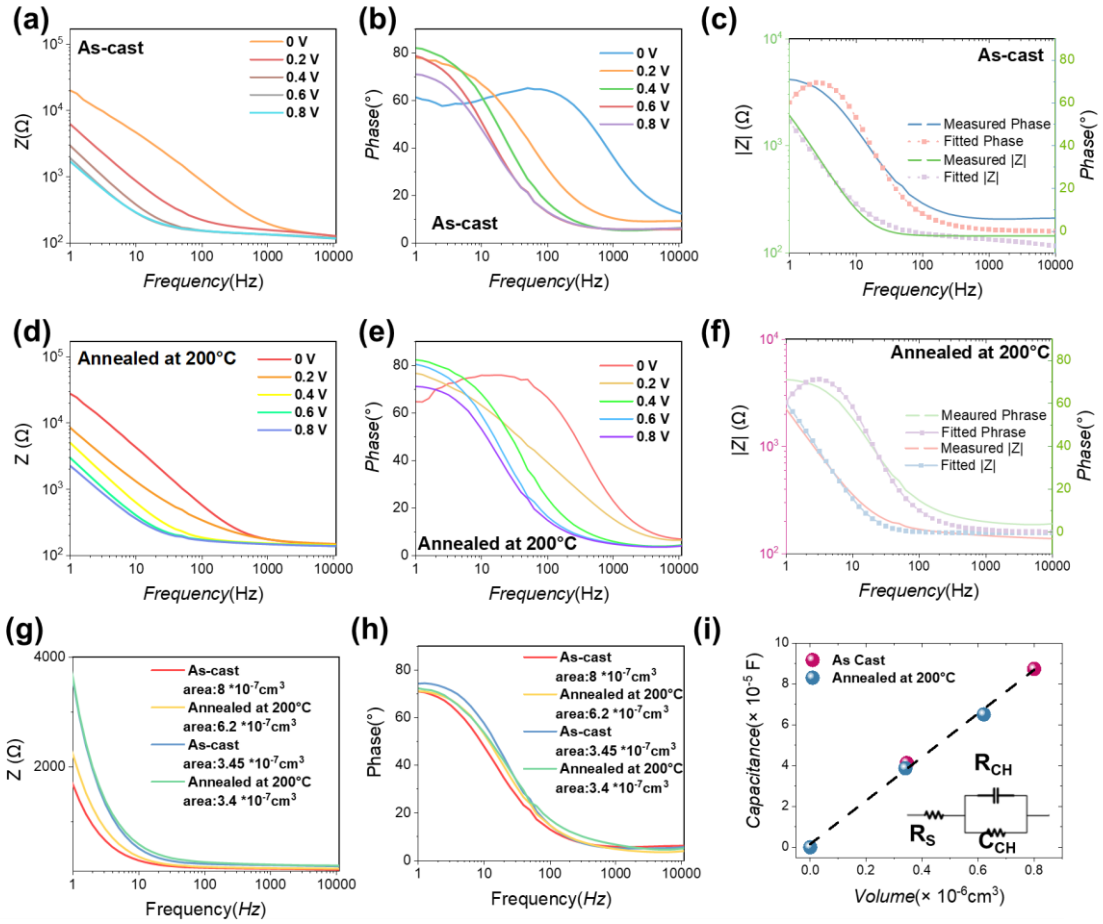

Figure S5. Electrochemical Bode plots of (a),(d) impedance, (b)(e) phase with potential bias (V_{bias}) vs. Ag/AgCl varying from 0 to 0.8 V and (c),(f) fitting using Randles circuit model at V_{bias}=0V for as-cast and annealed at 200 °C PBBTL films. Pt wire was used as the counter electrode, Ag/AgCl was used as the reference electrode, 0.1M NaCl was used as the electrolyte. (g) impedance and (h) phrase with potential bias (V_{bias}) vs. Ag/AgCl of 0.8V under different area and anneal condition. (i) linear fitting of volume v.s. capacitance extracted from Randles circuit model. In Randles circuit model, the R_S represents the resistance of the aqueous electrolyte, parallel connected R_{CH} and C_{CH} represents the resistance and capacitance of semiconducting polymer channel, respectively. The C* was normalized by dividing the volume of the thin film.

Table S1 OECT performance comparison under various anneal condition

Anneal condition	I_{ds} (V_{gs}=0.6 V) (μA)	g_m (μS)	μC^* (F cm^{-1}V^{-1} s^{-1})	V_{th} (V)	Stability	C* (F/cm^3)
As-cast	10.6	118	4.31±1.28	-0.41	76%	114.48
Annealed at 50 °C	8.5	86	3.61±0.99	-0.41	76%	NA
Annealed at 100 °C	6.4	69	3.72±1.13	-0.42	78%	NA
Annealed at 200 °C	4.9	75	3.62±1.48	-0.46	105%	108.41

Table S2 Detail comparison of EIS simulation results under different thermal annealing condition.

Sample	C (μF)	W (cm)	L (cm)	Thickness (nm)	C* (F/cm^3)	Average C*
As-cast-1	87.4	0.5	0.2	80	109.25	114.48
As-cast-2	41.3	0.37	0.1	92	119.71	
Annealed at 200°C -1	65.1	0.5	0.2	62	105	108.41
Annealed at 200°C -2	38.7	0.5	0.1	68	113.82	

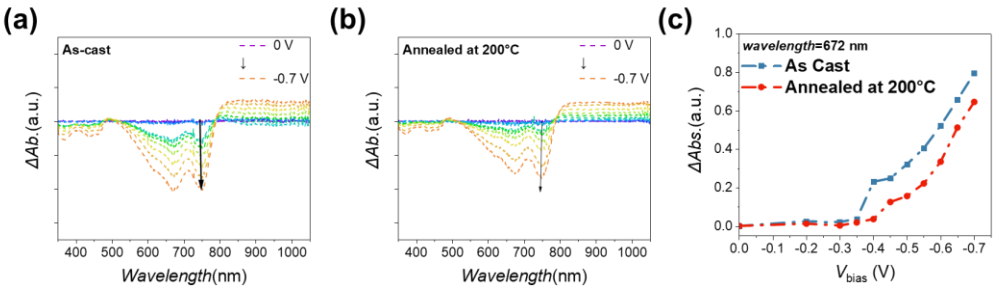

Figure S6 Absorption variation of PBBTL film under (a) as-cast and (b) annealed at 200 °C condition with bias varying from 0 to -0.7 V vs an Ag/AgCl electrode, at a step of 0.05 V, in 0.1M NaCl. (c) Ratio of absorption change of the as-cast and annealed PBBTL samples at 672 nm.

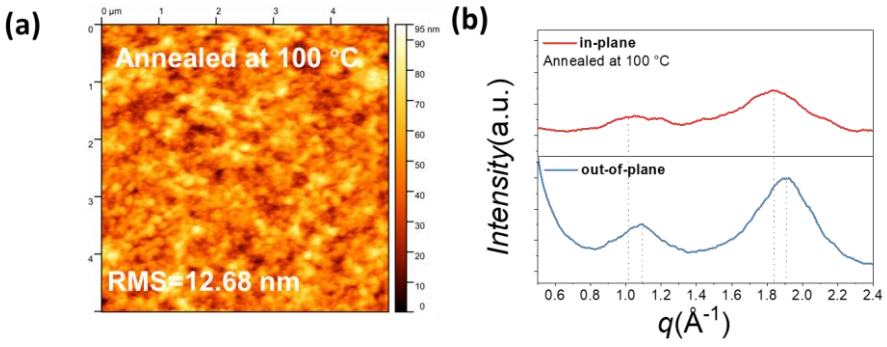

Figure S7 (a) AFM image of anneal PBBTL film at 100 °C (b) in-plane and out-of-plane line cut of the annealed PBBTL thin film at 100 °C.

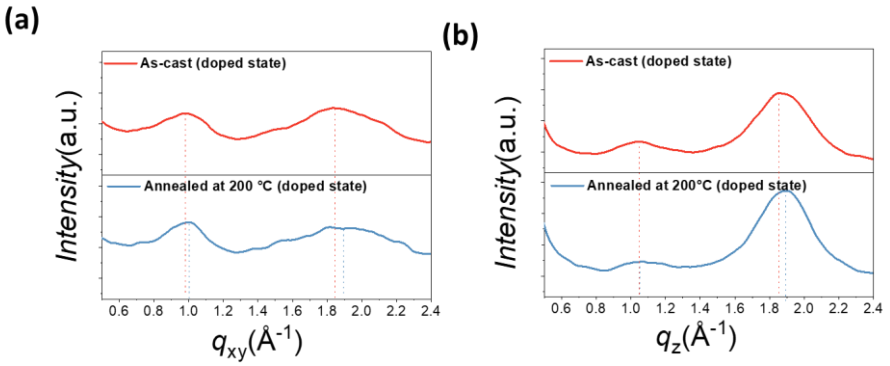

Figure S8 (a) In-plane and (b) out-of-plane line cut of the doped as-cast and annealed PBBTL thin films at 200 °C. The doped state was implemented by a 1500 cycling test (1s with 50 duty cycle) followed by a 200 s constant pulse of -0.6V.

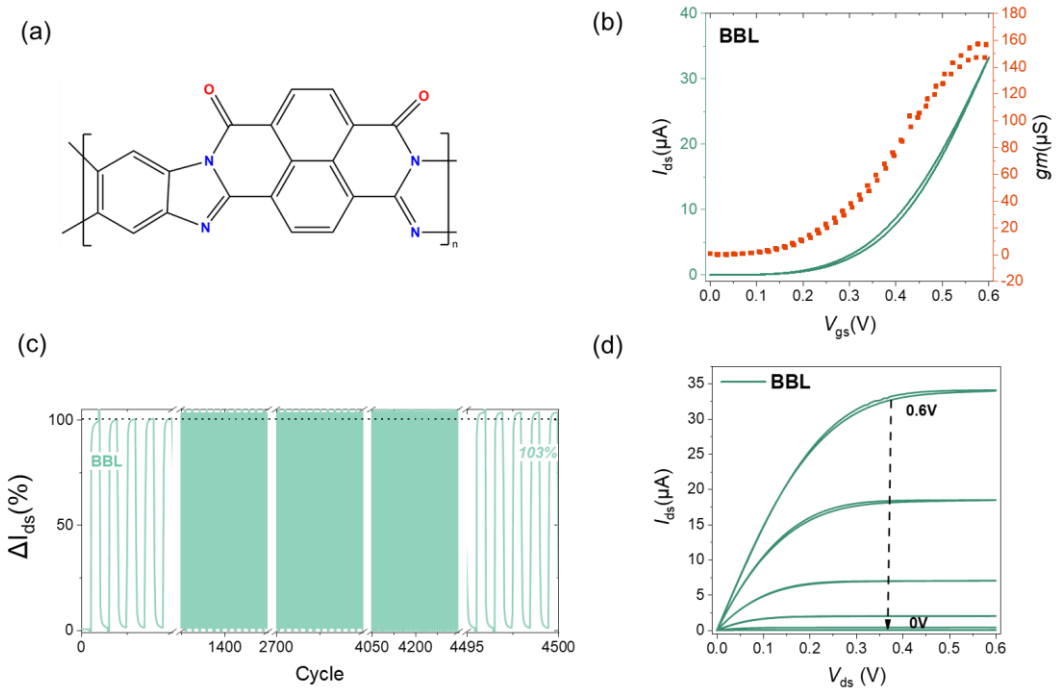

Figure S9 (a) Molecular structure of BBL (b) Transfer and transconductance characteristics of BBL OECT with 0.1 M NaCl aqueous electrolyte and V_{ds}= 0.6V. (c) Pulse stability of under ambient condition of BBL OECT with V_{gs} cycling between 0V to 0.6V, V_{ds} =0.6V, period of 0.4s with 50 % duty cycle. (d) Output characteristics of BBL OECT.

Table S3 Gain and power consumption comparison between this work and peer published work

Reference	V_{DD} (V)	*Gain* (V/V)	P (μW)	Technology
[9]	-9	30	1350	Unipolar
[30]	-2	9.5	20	Unipolar
[31]	-6	12	3270	Unipolar
[32]	5	14.59	16.14	Unipolar
[33]	0.6	90	0.7	Hybrid
[15]	0.6	69	0.71	Complementary
[16]	0.6	20	1.6	Complementary
[34]	0.6	26	15	Complementary
[35]	0.6	16	0.95	Complementary
This Work	**0.6**	**67**	**0.17**	**Complementary**

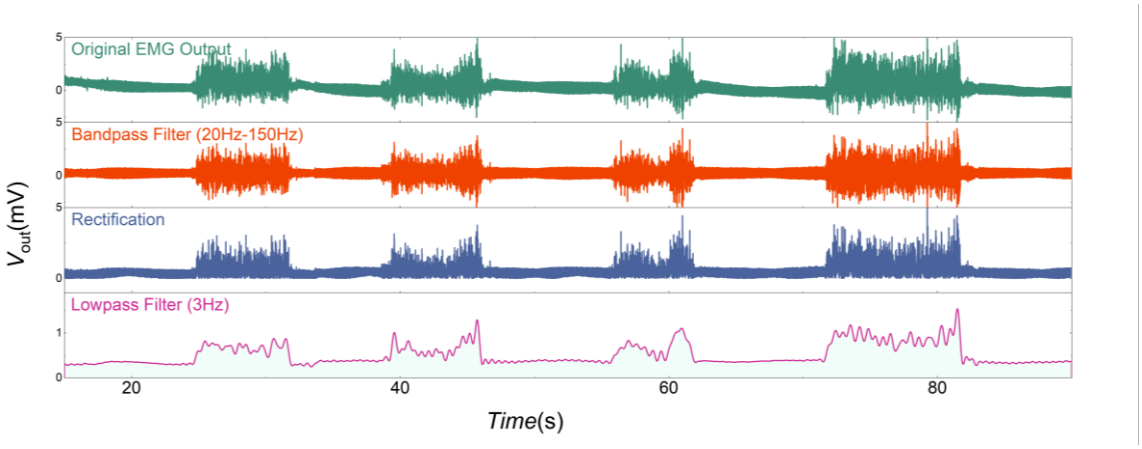

Figure S10 Original EMG with the processed results, including bandpass filter, rectification, and lowpass filter to extract the envelope.

The original EMG signal was collected by connecting the arm to a Keysight B2192A source meter(green line of **FigureS11**). As the arm swing angle increased, we observed an obvious enhancement in the absolute variation and envelope of the original EMG signal. Similarly, the amplified output displayed comparable results. The inverter responded to varying angles: a larger angle carries with a larger envelope, corresponded to higher changes in voltage. This indicates a correlation between the arm swing angle and the electrical signal, validating the effectiveness of our system in monitoring and reflecting changes in the EMG signal.

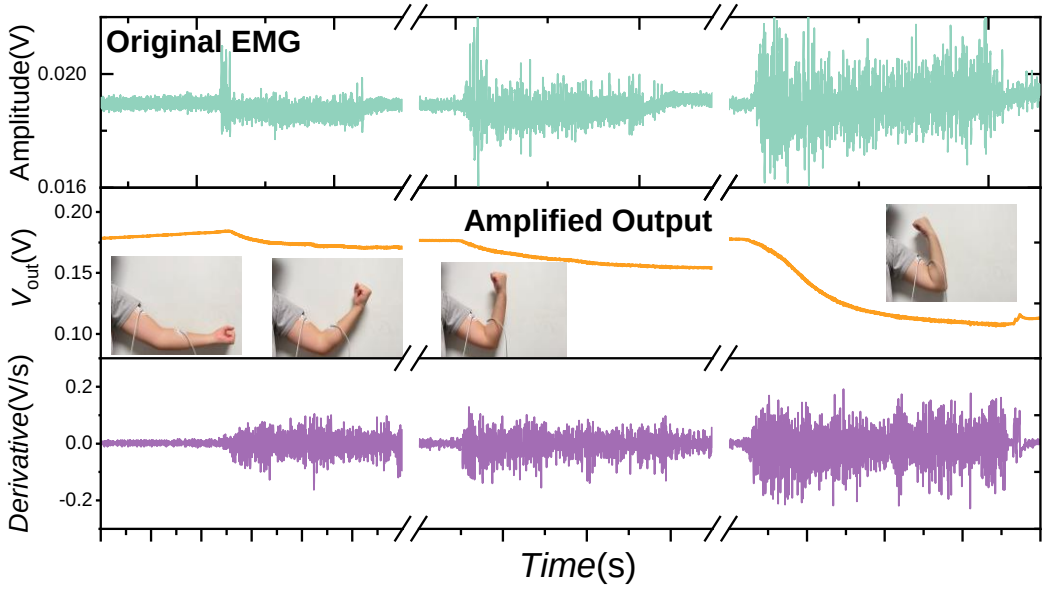

Figure S11 Quantitative analysis between the arm swing angle and amplitude of inverter output, with original EMG signal as a reference.

We also conducted a quantitative study examining the relationship between pulse duration and amplitude. We found that as the pulse duration extended, the variation in amplitude became larger. Interestingly, the output seemed to retain information on different pulse numbers, as shown in **Figure S12**. This suggests that our system may have potential applications in more complex signal processing tasks, further demonstrating its versatility and effectiveness.

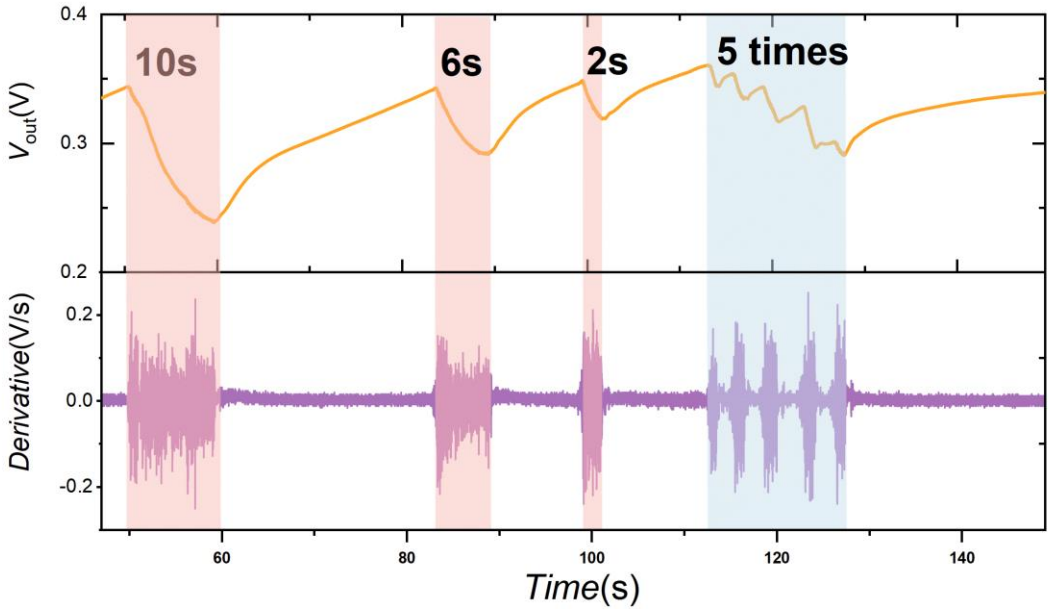

Figure S12 Quantitative analysis between the pulse duration and amplitude of inverter output.

Reference:

[9] M. Braendlein, T. Lonjaret, P. Leleux, J. M. Badier, G. G. Malliaras, *Adv. Sci.* **2017,** 4, 1600247.

[15] H. Y. Wu, C. Y. Yang, Q. Li, N. B. Kolhe, X. Strakosas, M. A. Stoeckel, Z. Wu, W. Jin, M. Savvakis, R. Kroon, D. Tu, H. Y. Woo, M. Berggren, S. A. Jenekhe, S. Fabiano, *Adv. Mater.* **2022**, 34, 2106235.

[16] C. Y. Yang, D. Tu, T. P. Ruoko, J. Y. Gerasimov, H. Y. Wu, P. C. Harikesh, M. Massetti, M. A. Stoeckel, R. Kroon, C. Müller, M. Berggren, S. Fabiano, *Adv. Electron. Mater.* **2022**, 8, 2100907.

[30] V. Venkatraman, J. T. Friedlein, A. Giovannitti, I. P. Maria, I. McCulloch, R. R. McLeod, J. Rivnay, *Adv. Sci.* **2018**, 5, 1800453.

[31] J. Rivnay, P. Leleux, M. Sessolo, D. Khodagholy, T. Herve, M. Fiocchi, G. G. Malliaras, *Adv. Mater.* **2013**, 25, 7010.

[32] M. Zabihipour, D. Tu, J. Strandberg, M. Berggren, I. Engquist, P. Andersson Ersman, *Adv. Mater. Technol.* **2021**, 6, 210055

[33] Y. Yao, W. Huang, J. Chen, G. Wang, H. Chen, X. Zhuang, Y. Ying, J. Ping, T. J. Marks, A. Facchetti, *Proc, Natl, Acad, Sci., U. S. A*. **2021**, 118.

[34] P. C. Harikesh, C. Y. Yang, D. Tu, J. Y. Gerasimov, A. M. Dar, A. Armada-Moreira, M. Massetti, R. Kroon, D. Bliman, R. Olsson, E. Stavrinidou, M. Berggren, S. Fabiano, *Nat Commun* **2022**, 13, 901.

[35] S. Zhang, M. Massetti, T. P. Ruoko, D. Tu, C. Y. Yang, X. Liu, Z. Wu, Y. Lee, R. Kroon, P. O. Å. Persson, H. Y. Woo, M. Berggren, C. Müller, M. Fahlman, S. Fabiano, *Adv. Funct. Mater.* **2021**, 32, 2106447.